

A LY α EMITTER WITH AN EXTREMELY LARGE REST-FRAME EQUIVALENT WIDTH OF $\sim 900\text{\AA}$ AT $Z = 6.5$: A CANDIDATE OF POPULATION III-DOMINATED GALAXY?¹

NOBUNARI KASHIKAWA^{2,3}, TOHRU NAGAO^{4,5}, JUN TOSHIKAWA³, YOSHIFUMI ISHIZAKI³, EIICHI EGAMI⁶, MASAO HAYASHI², CHUN LY^{7,12}, MATTHEW A. MALKAN⁸, YUICHI MATSUDA⁹, KAZUHIRO SHIMASAKU¹⁰, MASANORI IYE^{2,3}, KAZUAKI OTA⁴, TAKATOSHI SHIBUYA³, LINHUA JIANG⁶, YOSHIAKI TANIGUCHI¹¹, AND YASUHIRO SHIOYA¹¹

Received 2012 July 31; accepted 2012 October 15

ABSTRACT

We have identified a very interesting Ly α emitter, whose Ly α emission line has an extremely large observed equivalent width of $EW_0 = 436_{-149}^{+422}\text{\AA}$, which corresponds to an extraordinarily large intrinsic rest-frame equivalent width of $EW_0^{int} = 872_{-298}^{+844}\text{\AA}$ after the average intergalactic absorption correction. The object was spectroscopically confirmed to be a real Ly α emitter by its apparent asymmetric Ly α line profile detected at $z = 6.538$. The continuum emission of the object was definitely detected in our deep z' -band image; thus, its EW_0 was reliably determined. Follow-up deep near-infrared spectroscopy revealed emission lines of neither He II $\lambda 1640$ as an apparent signature of Population III, nor C IV $\lambda 1549$ as a proof of active nucleus. No detection of short-lived He II $\lambda 1640$ line is not necessarily inconsistent with the interpretation that the underlying stellar population of the object is dominated by Population III. We found that the observed extremely large EW_0 of the Ly α emission and the upper limit on the EW_0 of the He II $\lambda 1640$ emission can be explained by population synthesis models favoring a very young age less than 2 – 4 Myr and massive metal-poor ($Z < 10^{-5}$) or even metal-free stars. The observed large EW_0 of Ly α is hardly explained by Population I/II synthesis models with $Z \geq 10^{-3}$. However, we cannot conclusively rule out the possibility that this object is composed of a normal stellar population with a clumpy dust distribution, which could enhance the Ly α EW_0 , though its significance is still unclear.

Subject headings: cosmology: observation — early universe — galaxies: high-redshift — galaxies: formation

1. INTRODUCTION

Big-bang nucleosynthesis could not produce elements heavier than lithium at the beginning, while today we live in a universe with 90 kinds of constituent natural elements. It is thought that the universe was first metal enriched by the first generation of stars, Population III (Pop III) stars. Moreover, Pop III may have played a key role in cosmic reionization, and observational constraints

on their properties will significantly help the theoretical model to predict their characteristics as well as the quantity of ionizing photons produced by these first stars.

The observational characteristics to identify the first stars have been discussed by Tumlinson et al. 2001, Bromm et al. 2001, Oh et al. 2001, Schaerer 2002, Schaerer 2003, and Tumlinson et al. 2003. The first stars were born in an extreme condition with a metal-free, and presumably top-heavy initial mass function (IMF), though it held much in doubt by recent simulations (e.g., Krumholz et al. 2009, Turk et al. 2009, Stacy et al. 2012, Hosokawa et al. 2011). Their metal ejection to the intergalactic medium (IGM) may have caused a significant change in subsequent star formation. In the pristine gas cloud with low metallicities $Z \leq Z_{crit} = 10^{-5 \pm 1} Z_{\odot}$, molecules such as H₂ or HD dominated the cooling. Since zero-metal Pop III stars cannot burn in the CNO cycle like normal massive stars, their energy production has to rely initially on inefficient proton-proton burning. Therefore these stars have higher core temperatures of $\sim 10^8\text{K}$, which makes them hotter and smaller than their metal-enriched counterparts. Given the exceptionally high effective temperatures of Pop III stars in the zero-age main sequence, they emit a larger fraction of the luminosity in the Lyman continuum and have a much harder ionizing spectrum than stars with higher metallicity. The main characteristics of the predicted spectral energy distribution (SED) are the presence of a strong Ly α emission line due to the strong ionizing flux and a He⁺ recombination line (especially He II $\lambda 1640$) due to spectral hardness.

Despite great progress in the theoretical prediction of the unique physical properties of Pop III, direct observa-

Electronic address: n.kashikawa@nao.ac.jp

¹ Based on data collected at the Subaru Telescope, which is operated by the National Astronomical Observatory of Japan, and the W. M. Keck Observatory, which is operated as a scientific partnership among the California Institute of Technology, the University of California, and the National Aeronautics and Space Administration. The Observatory was made possible by the generous financial support of the W. M. Keck Foundation.

² Optical and Infrared Astronomy Division, National Astronomical Observatory, Mitaka, Tokyo 181-8588, Japan.

³ Department of Astronomy, School of Science, Graduate University for Advanced Studies, Mitaka, Tokyo 181-8588, Japan.

⁴ Department of Astronomy, Graduate School of Science, Kyoto University, Kyoto 606-8502, Japan.

⁵ The Hakubi Center for Advanced Research, Kyoto University, Kyoto 606-8302, Japan.

⁶ Steward Observatory, University of Arizona, 933 North Cherry Avenue, Tucson, Arizona 85721, USA

⁷ Space Telescope Science Institute, 3700 San Martin Drive, Baltimore, MD 21218.

⁸ Department of Physics and Astronomy, University of California, Los Angeles, CA 90095-1547.

⁹ Radio Astronomy Division, National Astronomical Observatory, Mitaka, Tokyo 181-8588, Japan.

¹⁰ Department of Astronomy, University of Tokyo, Hongo, Tokyo 113-0033, Japan.

¹¹ Research Center for Space and Cosmic Evolution, Ehime University, Bunkyo-cho, Matsuyama 790-8577, Japan.

¹² Giacconi fellow.

tional detection of Pop III stars has yet to be achieved. Based on a model prediction of Pop III abundances (Scannapieco et al. 2003), it is suggested that part of Pop III may have already been detected in ongoing surveys for high- z Lyman- α emitters (LAEs). There is indirect observational evidence for the existence of Pop III. A relatively high median value ($\sim 240\text{\AA}$) was derived from the rest-frame equivalent width (EW_0)¹³ distribution of LAEs at $z = 4.5$ (Malhotra & Rhoads 2002). However, the observational estimate of EW_0 at high- z is quite uncertain, because the continuum emission is faint or non-detected. A weak He II emission signature was detected in the composite spectrum of Lyman-break galaxies at $z \sim 3$ (Jimenez & Haiman 2006; Shapley et al. 2003) and $z \sim 4$ (Jones et al. 2012), although in these composite spectra, the expected nebular He II feature is indistinguishable from the stellar wind origin associated with evolved massive stars. Inoue et al. (2011) found some LAEs at $z = 3.1$ with extremely strong Lyman continuum flux, which can be explained by a very young and massive metal-poor or metal-free stellar population, if the mass fraction of such a population is $\sim 1-10\%$ of the total stellar mass of the LAEs. More straightforward but challenging attempts have failed to obtain direct evidence of Pop III, identifying simultaneously both Ly α and He II emissions in an individual spectrum (Nagao et al. 2005; Cai et al. 2011) or using a couple of narrow-band filters whose wavelengths are matched to the redshifted Ly α and He II emissions (Nagao et al. 2008).

We have found a very plausible Pop III candidate, which has an extraordinary large intrinsic EW_0^{int} ¹⁴ of $\sim 900\text{\AA}$ in the Ly α emission line at $z \sim 6.5$. Such an enormous $EW_0^{int} \sim 900\text{\AA}$ in the Ly α emission cannot be attained by the Population II synthetic cluster, and it is expected to be achieved by Pop III (with a Salpeter IMF up to $100M_\odot$) stars with young ages (Schaerer 2003; Tumlinson et al. 2003). Based on these models, the expected EW_0 of the He II emission should be as large as $\sim 100\text{\AA}$ for the object. In this study, we take a deep NIR spectroscopy for the candidate to verify its redshifted He II $\lambda 1640$ emission line at 12362\AA as firm evidence of a Pop III-dominated object. The detection of He II emission on the spectrum of this object will definitely provide the direct evidence of a Pop III-dominated object, as well as information about the critical epoch when the universe began to be enriched by metals. He II detection with a secure Ly α EW_0 estimate will have a strong impact on theoretical predictions about IMF, metallicity and the age of the metal-poor population. The feedback effects from Pop III would deeply affect subsequent star-formation, initial galaxy-formation, and IGM evolution (e.g., Ciardi et al. 2007).

An alternative interpretation of a large Ly α EW_0 is that the target has a large AGN contribution. We could clearly distinguish the AGN interpretation from a Pop III origin by identifying the C IV $\lambda 1549$ emission line as an apparent AGN signature at 11676\AA along with He II. The AGN fraction of the high- z LAE population at $z = 6.5$ is also an important question (Dijkstra & Wyithe 2006, Wang et al. 2004). The He II line can also origi-

nate in the hot, dense stellar winds of Wolf-Rayet stars, although the expected He II EW_0 would be small (e.g., 2.7\AA in the case of Erb et al. 2010) compared with the predictions of Pop III stars. In the case, detection of a broad He II line ($v_{\text{FWHM}} \sim 1500\text{km s}^{-1}$) and a simultaneous stronger C IV $\lambda 1549$ emission line with a P-Cygni profile would be expected (Leitherer et al. 1995). Otherwise, the large Ly α EW_0 could be the result of scattering in a clumpy, dusty medium (Neufeld 1991; Hansen & Oh 2006).

This paper is organized as follows: In § 2, we describe the photometric and spectroscopic identification of the candidate, and its Ly α EW_0 estimate. In § 3, we describe our deep NIR spectroscopic observation aimed at detecting its He II $\lambda 1640$ or C IV $\lambda 1549$ emissions. In § 4, we present the measurements of flux upper limits on these lines. Several possible interpretations of the observed large Ly α EW_0 are discussed in § 5. A summary of the paper is provided in § 6, with some discussion of the implications of our results.

Throughout the paper, we assume cosmology parameters: $\Omega_m = 0.3$, $\Omega_\Lambda = 0.7$, and $H_0 = 70 h_{70} \text{ km s}^{-1} \text{ Mpc}^{-1}$. These parameters are consistent with recent CMB constraints (Komatsu et al. 2009). Magnitudes are given in the AB system.

2. THE CANDIDATE AND ITS LY α EQUIVALENT WIDTH

2.1. Optical Spectroscopy

The object with a large Ly α EW, SDF-LEW-1, was discovered in the course of our systematic large spectroscopic survey of LAEs at $z = 6.5$ (Kashikawa et al. 2006, 2011) in the Subaru Deep Field (SDF). We have identified a total of 43 spectroscopically confirmed LAEs at $z = 6.5$ (Kashikawa et al. 2011). The sample was based on the flux excess objects in the narrowband NB921 ($\lambda_c = 9196 \text{\AA}$, FWHM=132 \AA) image, compared with the deep broadband images of the SDF. SDF-LEW-1 was first spectroscopically confirmed to be a real LAE by Subaru/FOCAS observation on May 20-21 2007, though the quality of spectra was not good due to poor conditions. The object was re-observed by Keck/DEIMOS on April 27, 2009. The integration time was 10.8ksec with a seeing size of $0.''7$. The object shows an apparent asymmetric Ly α line profile detected at $z = 6.538$ ¹⁵(Figure 1). To quantitatively estimate the line asymmetry, we introduce the weighted skewness parameter, S_W (Kashikawa et al. 2006), which is defined as the third moment of flux distribution multiplied by the line width. The S_W of SDF-LEW-1 is estimated to be $S_W = 9.33 \pm 0.27$, which is larger than the empirical critical value of $S_W = 3\text{\AA}$ to distinguish Ly α emission from other emission lines at $z > 5.7$. The clear asymmetry of the emission line ensures that it is certainly a Ly α emission, distinct from foreground nebular emissions. The high resolving power of DEIMOS can distinguish a single Ly α emission from [O II] doublets (at a rest-frame separation of 2.78\AA), and the absence of any other emission line features both in the optical, and the NIR spectrum, as will be shown later

¹³ We refer to the rest-frame equivalent width, which is a factor of $(1+z)$ lower than the observed equivalent width.

¹⁴ We refer to the IGM-attenuation corrected EW_0 .

¹⁵ The spectroscopic properties of the object, SDF J132458.0+272349, are slightly different from those listed in Table 2 of Kashikawa et al. (2011), which is based on the previous Subaru/FOCAS low-quality spectrum. We use measurements based on the DEIMOS observation throughout this paper.

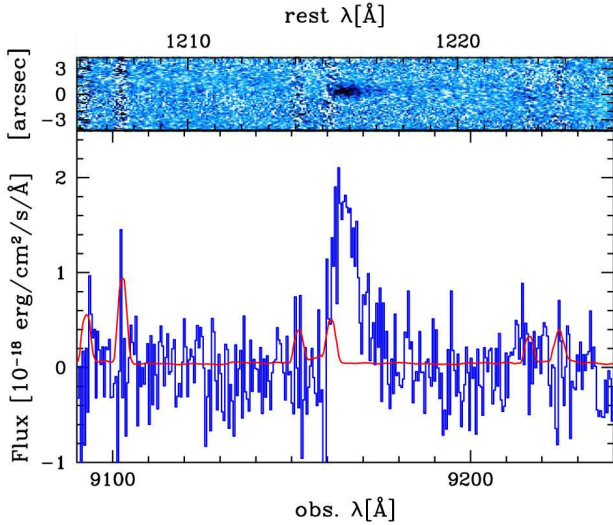


FIG. 1.— Two-dimensional (upper) and one-dimensional (lower) optical spectrum of SDF-LEW-1. Red line represents sky lines.

In Section 4, rules out the possibility of its being some other emission line, such as $H\alpha$, $H\beta$, and $[O\ III]$. It has a total $Ly\alpha$ luminosity of $(1.07 \pm 0.30) \times 10^{43}$ erg s $^{-1}$. This corresponds to a $Ly\alpha$ -based star formation rate (SFR) of $9.7 M_{\odot}$ yr $^{-1}$ using $SFR(Ly\alpha) = 9.1 \times 10^{-43} L(Ly\alpha) M_{\odot}$ yr $^{-1}$ (Kennicutt 1998), though it is more or less affected by uncertainties of dust extinction, IMF, and $Ly\alpha$ escape fraction.

2.2. EW_0 measurement

EW_0 was calculated as in Kashikawa et al. (2011), using narrow- ($NB921$) and broad-band (z') photometry taking into account the non top-hat shape bandpass, which potentially has substantial consequences in deriving line and continuum fluxes (Gronwall et al. 2007). We assumed a simple model spectrum with constant UV continuum and $Ly\alpha$ emission line, including complete IGM absorption at the blue ward of $Ly\alpha$. The $Ly\alpha$ emission flux, $f^{phot}(Ly\alpha)$, and the UV continuum flux density at the $Ly\alpha$ wavelength $f_{cont}^{phot}(0.92\mu m)$, can be separately estimated by fitting the model spectrum to the observed fluxes in the narrow-band and the z' -band. Table 1 summarizes the photometry, and Figure 2 shows thumbnail images of SDF-LEW-1. SDF-LEW-1 was only detected in $NB921$ - and z' -band images, and it was below the 3σ limiting magnitude at other wavelengths. The errors in these photometrical fluxes are estimated in the same way as Kashikawa et al. (2011), in which Gaussian random photometric errors in both the narrow- and broad-band were assigned to the measured magnitudes. The rms fluctuations of the fluxes are estimated from a Monte Carlo simulation. Although we obtained multi-wavelength photometric data for the object, it is difficult to put a meaningful constraint on its stellar population, even for its stellar mass, by SED fitting because the object is detected only in $NB921$ - and z' -band images. We confirmed that the photometrically determined $Ly\alpha$ emission flux, $f^{phot}(Ly\alpha) = 2.34_{-0.06}^{+0.06} \times 10^{-17}$ ergs s $^{-1}$

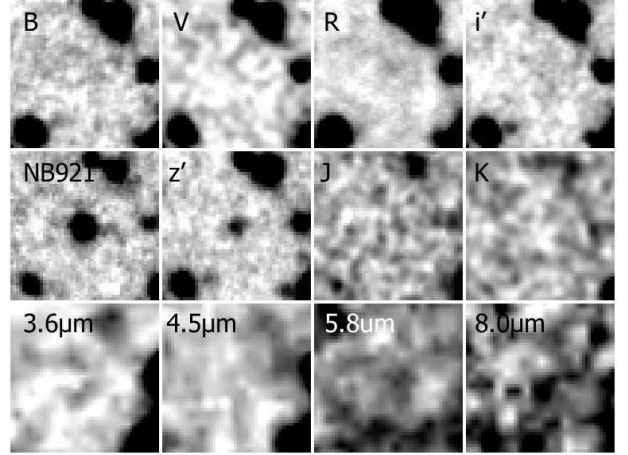


FIG. 2.— Thumbnail images of SDF-LEW-1. The B , V , R , i' , $NB921$, z' , J , K , $3.6\mu m$, $4.5\mu m$, $5.8\mu m$, and $8.0\mu m$ -band images are shown from upper-left to lower-right. Each image is $10''$ on a side. North is up, and east is to the left. A constant gray level corresponds to constant f_{ν} surface brightness.

cm $^{-2}$, is fairly consistent with that measured in the optical spectrum, $f_{opt}^{spec}(Ly\alpha) = (2.19 \pm 0.62) \times 10^{-17}$ ergs s $^{-1}$ cm $^{-2}$, where errors only reflect spectroscopic rms uncertainties. Simultaneously, the UV continuum emission flux density at $Ly\alpha$ wavelength is estimated to be $f_{cont}^{phot}(0.92\mu m) = (7.12 \pm 3.41) \times 10^{-21}$ ergs s $^{-1}$ cm $^{-2}$ \AA^{-1} , though its flux is as small as 2σ level. This implies that most of the z' -band flux would be contributed by the $Ly\alpha$ flux. Therefore, the EW_0 of SDF-LEW-1 is estimated to be 436_{-149}^{+422} \AA . We here assumed the continuum SED to be $f_{\lambda} \propto \lambda^{\beta}$ and $\beta = -2.0$. Finkelstein et al. (2011c) found that the UV continuum slope β of Lyman Break Galaxies (LBGs) evolves significantly from $\beta = -1.83$ at $z = 4$ to -2.37 at $z = 7$, and that fainter galaxies have steeper β , while Dunlop et al. (2012) concluded a constant $\beta \sim -2.0$ at $z = 5 - 7$, irrespective of redshift and UV magnitude. Ouchi et al. (2008) concluded that β of LAEs, which are generally less dusty and/or younger, is slightly smaller than those of LBGs. When we changed the assumption $\beta = -2.0$ to $\beta = -2.5$ (-1.5), we found that $f_{cont}^{phot}(0.92\mu m)$ varies as 7.01 ± 3.44 (7.24 ± 3.56) $\times 10^{-21}$ ergs s $^{-1}$ cm $^{-2}$ \AA^{-1} . The possible scatter of $f_{cont}^{phot}(0.92\mu m)$ due to the β assumption is smaller than its internal error. We also found that $f^{phot}(Ly\alpha)$ remains unchanged for various assumed values of beta.

It is particularly worth noting that the object has an extremely large EW_0 of 436_{-149}^{+422} \AA , which is exceptionally larger than those of other LAEs at $z = 6.5$ (Kashikawa et al. 2011) and at lower- z (Shimasaku et al. 2006; Gronwall et al. 2007; Ouchi et al. 2008). For example, Gronwall et al. (2007) showed that the EW_0 distribution of LAE at $z = 3.1$ follows an exponential curve with an e-folding scale length of 76_{-8}^{+11} \AA . Several Pop III candidates with $Ly\alpha$ EW_0 as large as ~ 100 – 300 \AA have been identified in previous works (e.g., Malhotra & Rhoads 2002), though most of their EW_0 were only given by a lower limit because their continuum emissions were not detected in broad-band images. Adams et al. (2011) found three LAEs with $EW_0 > 240$ \AA among their wide-field HETDEX (Hobby-Eberly

TABLE 1
 PHOTOMETRY OF SDF-LEW-1

B	V	R	i'	$NB921$	z'	J	K	$3.6\mu\text{m}$	$4.5\mu\text{m}$	$5.8\mu\text{m}$	$8.0\mu\text{m}$
> 28.58	> 27.85	> 28.35	> 27.72	24.69 ± 0.024	26.93 ± 0.082	> 24.74	> 24.13	> 25.67	> 25.90	> 23.98	> 23.64

NOTE. — The lower limit denotes the 3σ limiting magnitude. The (limiting) magnitudes in optical and near-infrared bands are measured in $2''$ aperture, while those in mid infrared bands are measured in $2\times\text{FWHM}$ aperture. Refer to the photometric data descriptions to Kashikawa et al. (2004) (B , V , R , $NB921$), Poznanski et al. (2007); Graur et al. (2011) (i' , z'), Hasashi, M. et al. in prep., Toshikawa et al. (2012) (J , K), and Egami, E. et al. in prep. ($3.6\mu\text{m}$ - $8.0\mu\text{m}$).

Telescope Dark Energy Experiment) pilot spectroscopic survey, though one had no counterpart in the broad-band image, and the other two seemed to be extended Ly α blobs. High EW_0 objects with no counterparts in the broad-band cannot be distinguished from noise contaminations (Adams et al. 2011) or transient objects (Shibuya et al. 2012). However, SDF-LEW-1 was actually detected in the z' -band image by virtue of deep SDF imaging data, and its EW_0 was reliably determined. The 2nd largest EW_0 of our z' -detected LAE sample at $z = 6.5$ was $\text{EW}_0 = 152\text{\AA}$. It should be noted that the z' -band image, which was constructed from 30 hrs integration time in total by stacking all the data taken between 2001 and 2008, had a 3σ limiting magnitude as deep as 27.09 mag.

2.3. Estimate of intrinsic EW_0

It is well known that Ly α photons are easily absorbed by dust and H I clouds inside a galaxy. In our previous study (Kashikawa et al. 2006), we showed that the blue-side line profile of the Ly α emission of the composite spectrum of our LAE sample at $z = 6.5$ can be simply explained by spectral broadening alone, which means that the blue-side of the observed Ly α emission is almost completely absorbed. We confirmed that the blue-side of Ly α line profile of SDF-LEW-1 was also steep enough to be explained by simple spectral broadening (the instrumental resolution $\text{FWHM} = 2.5\text{\AA}$), though the spectral data quality of a single object was not good enough to accurately estimate the profile. This is expected from the IGM attenuation model by Madau (1995), which predicts only 2% transmission on the blue half of the Ly α emission line at $z = 6.5$. In this case, SDF-LEW-1 has an intrinsic EW_0^{int} of $872_{-298}^{+844}\text{\AA}$. The IGM/ISM absorption correction that we applied here is relatively large, and requires an enough attention on its uncertainty. It has been suggested that large-scale outflows are ubiquitous in LAEs with Ly α velocity offsets of $\Delta v_{\text{Ly}\alpha} \sim 100 - 300$ km/s (McLinden et al. 2011; Finkelstein et al. 2011a; Hashimoto et al. 2012) from the systemic redshift of the galaxy. The outflow forces Ly α photons to reach frequencies further from line center to escape; therefore in this case, smaller IGM correction is expected. For example, when assuming an intrinsically symmetric line profile with $\Delta v_{\text{Ly}\alpha} = 100$ km/s, only $\times 1.38$ correction instead of $\times 2$ should be applied for SDF-LEW-1. However, as discussed above, SDF-LEW-1 has a sharp blue edge of Ly α line profile, which is difficult to be reconciled with the strong outflow hypothesis (Orsi et al. 2012; Laursen et al. 2011). On the other hand, the entire Ly α line at redshifts during the reionization epoch may be suppressed by a damping wing of the neutral IGM along the line-of-sight (Haiman & Cen 2005). Therefore, the

estimate of EW_0^{int} might give only a lower-limit, if it was taken during the reionization epoch. For simplicity, we here assume that the IGM is almost completely ionized (the neutral fraction of IGM hydrogen, $x_{\text{HI}} \sim 0$) at $z \sim 6.5$. In addition, there are several uncertainties in deriving EW_0^{int} due to a possible variation of IGM attenuation from object to object and internal ISM attenuation. Although we hereafter use simple $\times 2$ correction, it should be noted that EW_0^{int} could have uncertainties, that are difficult to quantify, other than its observational errors.

The Ly α $\text{EW}_0^{\text{int}} \sim 900\text{\AA}$ of SDF-LEW-1 is far greater than those of almost all LAEs ever observed. Such an enormous $\text{EW}_0^{\text{int}} \sim 900\text{\AA}$ in the Ly α emission cannot be attained by Population II synthesis. Dijkstra & Wyithe (2007) also suggested that a Pop III contribution is inevitably required to self-consistently reproduce large EW_0 and observed Ly α /UV luminosity functions at $z = 6.5$ (Kashikawa et al. 2006). Although Pop III formation might continue down to $z = 2.5$, depending on feedback efficiency (Tornatore et al. 2007), the expected fraction of Pop III objects among LAE sample significantly increases with redshift (Scannapieco et al. 2003). The probability to find Pop III objects is expected to be 100 times larger at $z = 6.5$ than at $z \sim 3$. SDF-LEW-1, which has an extraordinary $\text{EW}_0^{\text{int}} \sim 900\text{\AA}$ at the high-redshift of $z = 6.5$, can easily convince us that it is a plausible Pop III candidate. The most promising way to identify this candidate as a Pop III dominant object is to directly detect its strong He II $\lambda 1640$ emission. The finding of such a rare object with a large EW_0 is really indebted to the Subaru wide-field data. The target is the only plausible and accessible Pop III candidate among the largest sample of spectroscopically identified LAEs at $z = 6.5$, which is very close to their birth epoch; *i.e.*, the end of the “dark age”. The He II lines suffer minimal effects of scattering by gas and decreasing attenuation by intervening dust. Moreover, the He II emission is expected to be detected at 12362\AA , which fortunately does not correspond to the wavelengths of any strong OH sky lines.

3. NIR SPECTROSCOPY

We took deep NIR spectroscopy for SDF-LEW-1 with Subaru/MOIRCS (Ichikawa et al. 2006) on April 15-16 2011 (UT). The observations were made with the $zJ500$ grism with a 0.8 arcsec slit width ($R \sim 450$). The spectra covered $0.9 - 1.8\mu\text{m}$, with a pixel resolution of 5.57\AA . We used MOS mode, which allows a more secure method of quickly and accurately aligning the slit on such a faint target, compared with the longslit mode in the case of MOIRCS. We used two masks, and both masks contained the target. The total integration time was 44.8

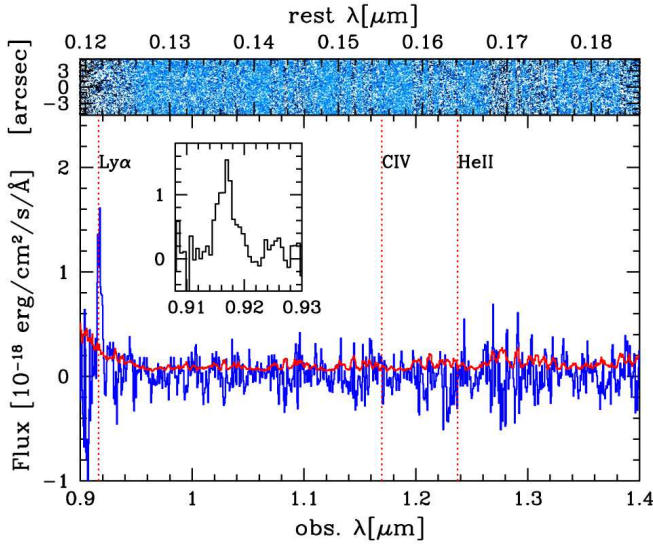


FIG. 3.— Two-dimensional (upper) and one-dimensional (lower) NIR spectrum of SDF-LEW-1. The vertical dotted lines indicate the wavelength of Ly α , C IV, and He II emission lines at $z = 6.538$. The 1σ error spectrum (red line) is overlaid. The inset panel shows the closeup of detected Ly α emission line.

ks (~ 12.44 hr), with a single exposure time of 500 – 900 sec, depending on the sky background level. During the observation, the telescope was nodded at two positions (A and B), with a dithering of $5.''0$ to achieve adequate background subtraction. The seeing size was ~ 1 arcsec. We obtained a spectrum of the spectrophotometric standard star Feige 34 for flux calibration. The data were reduced in a standard way using IRAF. The spatial position of the blind target of each exposure spectrum was carefully determined by dithering the pattern of other bright objects on other slits in the same mask. The final spectrum was constructed from the median frame with weights based on the relative flux transparency of each exposure, which was also measured from other bright objects in other slits.

4. RESULTS

The final spectrum is shown in Figure 3. The prominent Ly α emission was detected at 9169.6\AA , which is almost consistent with the optical spectrum shown in Figure 1, even at the bluest edge, where MOIRCS sensitivity drops significantly. S_W was estimated to be $S_W = 8.26 \pm 1.16$, demonstrating an apparent asymmetric Ly α line profile. The Ly α emission flux was estimated to be $f_{NIR}^{spec}(\text{Ly}\alpha) = (4.8 \pm 0.20) \times 10^{-17} \text{ ergs s}^{-1} \text{ cm}^{-2}$, which is higher than that measured in the optical spectrum. The absolute flux calibration of the NIR spectrum is unreliable at the bluest wavelength; therefore, we hereafter refer the spectroscopic Ly α emission flux to that measured in the optical spectrum.

No emission line feature is seen around $1.2362\mu\text{m}$, at which the He II $\lambda 1640$ emission is expected to appear, both on the one-dimensional (upper panel of Figure 4) and two-dimensional spectrum. Note that the expected wavelength of He II appearance is based on the redshift

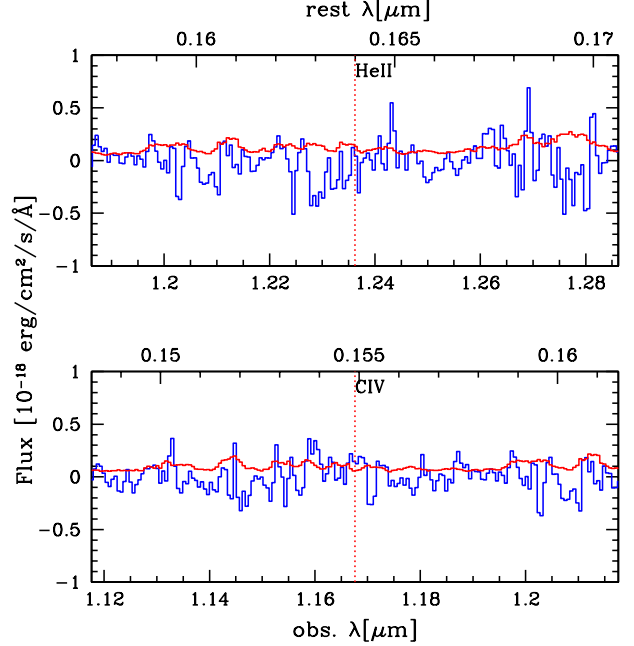


FIG. 4.— The closeup spectra around expected wavelength of He II (upper) and C IV (lower) at $z = 6.538$, respectively. The 1σ error spectrum (red line) is overlaid.

determined from the peak of the Ly α emission, which could be, however, offset to the red from the systemic redshift due to absorption, though the upper limits described below would not significantly change even in the case. The He II flux limits were derived using the $1.''0 \times 25.6\text{\AA}$ aperture, assuming that the He II line is expanded to almost seeing size and is unresolved. The 3σ upper limit on the He II flux from SDF-LEW-1 is $3.39 \times 10^{-19} \text{ ergs s}^{-1} \text{ cm}^{-2}$, which corresponds to a luminosity of $1.66 \times 10^{41} \text{ ergs s}^{-1}$. The UV continuum emission flux density at $1.2362\mu\text{m}$ is photometrically estimated to be $f_{cont}^{phot}(1.24\mu\text{m}) = (3.91 \pm 2.07) \times 10^{-21} \text{ ergs s}^{-1} \text{ cm}^{-2} \text{ \AA}^{-1}$ for $\beta = -2.0$, providing the 3σ upper limit on EW_0 of He II $\lambda 1640$ as $\leq 11.5_{-3.98}^{+12.9} \text{ \AA}$. The possible β uncertainty could change $f_{cont}^{phot}(1.24\mu\text{m})$ to 3.32 ± 1.64 (4.62 ± 2.41) $\times 10^{-21} \text{ ergs s}^{-1} \text{ cm}^{-2} \text{ \AA}^{-1}$, for $\beta = -2.5$ (-1.5). The uncertainty is still within the internal error of $f_{cont}^{phot}(1.24\mu\text{m})$ itself, though it is larger than in the case of $f_{cont}^{phot}(0.92\mu\text{m})$ due to a long extrapolation from the z' -band. Equivalently, the 3σ upper limit on the observed He II $\lambda 1640/\text{Ly}\alpha$ ratio is constrained to be 1.55×10^{-2} . The ratio could become much smaller if the observed Ly α was attenuated by either the interstellar or intergalactic medium. In the spectrum, the UV continuum flux was not detected with enough significance to measure its EW_0 spectroscopically. The 3σ upper limit flux density at $0.95\mu\text{m}$ is $6.24 \times 10^{-20} \text{ ergs s}^{-1} \text{ cm}^{-2} \text{ \AA}^{-1}$, which is higher than the photometric estimate. It is generally very difficult to measure the EW_0 of high- z LAEs from their spectroscopic data, because most LAEs are too faint to accurately determine their continuum flux on the spectra.

The C IV $\lambda 1549$ (lower panel of Figure 4) was neither detected around $1.1676\mu\text{m}$, where the 3σ upper limit constraint is $2.83 \times 10^{-19} \text{ ergs s}^{-1} \text{ cm}^{-2}$ with the same aperture size as in the case of He II, suggesting that the object

is not an apparent active AGN. $f_{cont}^{phot}(1.17\mu\text{m})$ was estimated to be $(4.39 \pm 2.17) \times 10^{-21} \text{ ergs s}^{-1} \text{ cm}^{-2} \text{ \AA}^{-1}$ for $\beta = -2.0$, and the 3σ upper limit on EW_0 of C IV $\lambda 1549$ is given by $\leq 8.55_{-2.82}^{+8.36} \text{ \AA}$.

5. DISCUSSION

In this section, we discuss a variety of possible mechanisms that can explain the extremely strong Ly α emission with $\text{EW}_0^{int} = 872_{-298}^{+844} \text{ \AA}$ and no detection of He II $\lambda 1640$ or C IV $\lambda 1549$ emissions from SDF-LEW-1.

5.1. Pop III

The large $\text{EW}_0^{int} = 872_{-298}^{+844} \text{ \AA}$ of the Ly α emission line of SDF-LEW-1 can be expected as an interesting characteristic of young, metal-poor or metal-free stellar populations in the first galaxies. The derived upper limit on the He II $\lambda 1640$ emission can constrain the IMF, metallicity, star formation history, and age of the population. We here compare the observed EW_0 of the Ly α emission as well as the upper limit on the He II emission with the model predictions of Raiter et al. (2010), which are the extended calculations of Schaerer (2003) and predict the EW_0 of these lines on the basis of their evolutionary synthesis code for a variety of different IMFs covering metallicities from zero to solar.

Figure 5 compares the predicted EW_0 of Ly α and He II $\lambda 1640$ as a function of age for models of constant star formation (CSFR) over 1 Gyr and young bursts ($< 4 \text{ Myr}$). We show six different IMF models: 1) Model-S, Salpeter IMF with stellar mass range $1 < M < 100 M_\odot$ (black); 2) Model-B, Salpeter IMF with $1 < M < 500 M_\odot$ (green, dashed); 3) Model-C, Salpeter IMF with $50 < M < 500 M_\odot$ (cyan, dashed); 4) Model-Sc, Scalo IMF with $50 < M < 500 M_\odot$ (blue); 5) Model-TA, log-normal IMF with $1 < M < 500 M_\odot$, $M_c = 10$, and $\sigma = 1.0$ as defined in Tumlinson (2006) (red); and 6) Model-TB, log-normal IMF with $1 < M < 500 M_\odot$, $M_c = 15$, and $\sigma = 0.3$ (magenta). The color codes for the different IMF models are the same as those used in Table 1 of Raiter et al. (2010). For simplicity, we did not show the results from their L05 and TE models, which are almost the same as those of the other models. Note that the Model-C evolutionary track is only available up to $\sim 4 \text{ Myr}$, because its IMF contains only massive stars. The horizontal orange lines with shaded regions indicate the observed constraints of the EW_0 (3σ upper limits for He II) and their error ranges.

Table 2 summarizes the acceptable age range in which each model can simultaneously explain the observed constraints of both Ly α and He II for each metallicity. Figure 5 exhibits the general trend that higher EW_0 are expected for both Ly α and He II lines at younger ages and lower metallicities. The maximum $\text{EW}_0 \sim 1500 \text{ \AA}$ and $\sim 90 \text{ \AA}$ for Ly α and He II can be attained with $Z = 0$, a very young age ($< 1 \text{ Myr}$), and IMFs favoring more massive stars. At zero-metallicity (the top panel of Figure 5), the large Ly α $\text{EW}_0^{int} = 872_{-298}^{+844} \text{ \AA}$ of SDF-LEW-1 can be explained by most of the IMF models at very young ages $< 4 \text{ Myr}$, and by some of the CSFR models (Model-S, B and TA) even at ages $> 4 \text{ Myr}$, while some models predict higher He II EW_0 than the observed upper limit at ages $< 1 \text{ Myr}$. All of the burst models have narrow age ranges, in which they are consistent with the constraints of both Ly α and He II. The CSFR S model at

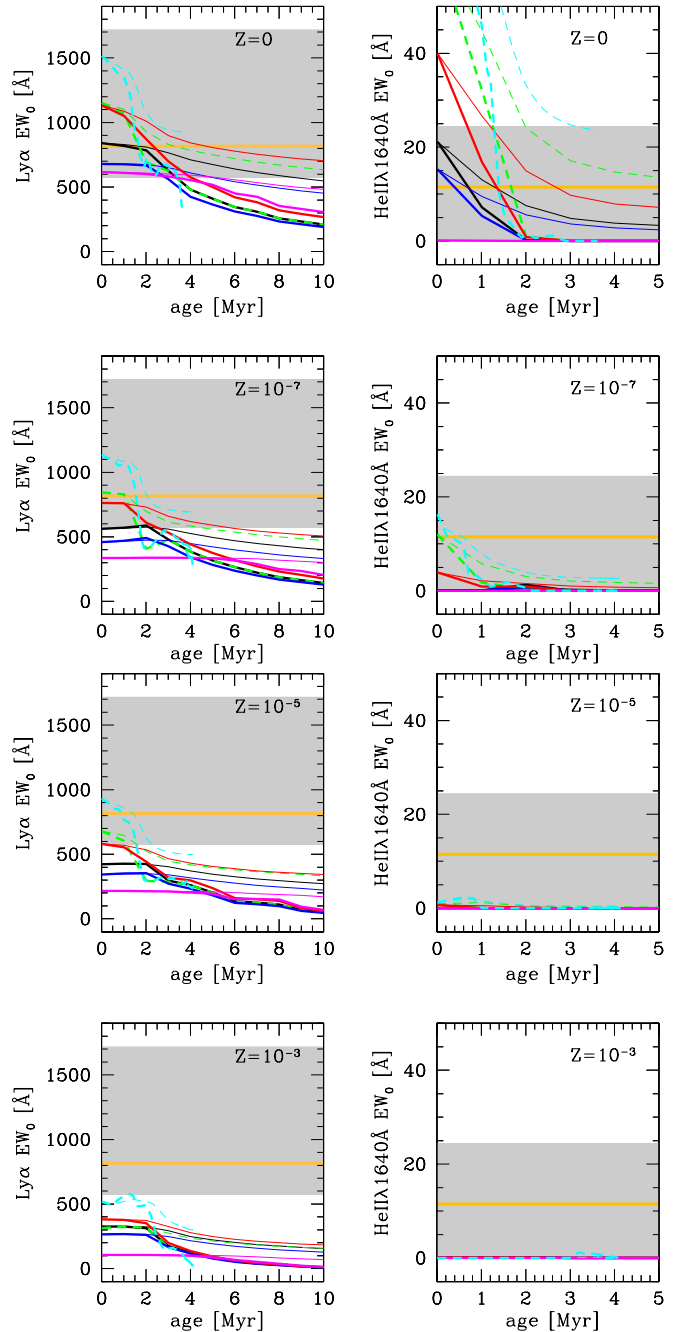


FIG. 5.— Predicted Ly α (left) and He II $\lambda 1640$ (right) EW_0 as a function of age (Myr) for constant star formation (thin line) and young bursts (thick) models. The color codes of different IMF models are the same as those in Table 1 of Raiter et al. (2010): *i.e.*, 1) Model-S, Salpeter IMF with stellar mass range $1 < M < 100 M_\odot$ (black); 2) Model-B, Salpeter IMF with $1 < M < 500 M_\odot$ (green, dashed); 3) Model-C, Salpeter IMF with $50 < M < 500 M_\odot$ (cyan, dashed); 4) Model-Sc, Scalo IMF with $50 < M < 500 M_\odot$ (blue); 5) Model-TA, log-normal IMF with $1 < M < 500 M_\odot$, $M_c = 10$, and $\sigma = 1.0$ as defined in Tumlinson (2006) (red); and 6) Model-TB, log-normal IMF with $1 < M < 500 M_\odot$, $M_c = 15$, and $\sigma = 0.3$ (magenta). For simplicity, we did not show the results from Model-L05 and Model-TE in Raiter et al. (2010), which are almost the same as those of the other models. The Model-C, which contains only massive stars above $50 M_\odot$, is calculated to the age $\approx 4 \text{ Myr}$. The horizontal orange lines with shaded regions indicate the observational constraint of EW_0 ($\text{EW}_0^{int} = 872_{-298}^{+844} \text{ \AA}$ for Ly α and $\leq 11.5_{-3.98}^{+12.9} \text{ \AA}$ for He II) and their error ranges.

TABLE 2
CONSTRAINTS ON RAITER ET AL.(2010)’S IMF MODELS

Z		0	10^{-7}	10^{-5}	10^{-3}
Model-S	burst	< 3.5Myr	< 2Myr	-	-
	CSFR	< 9Myr	< 2Myr	-	-
Model-B	burst	1.5 – 3.5Myr	< 1.5Myr	< 1Myr	-
	CSFR	2Myr<	< 4.5Myr	< 1.5Myr	-
Model-C	burst	1.5 – 3.5Myr	< 1.5Myr	< 1.5Myr	-
	CSFR	-	< 4Myr	< 2Myr	-
Model-Sc	burst	< 3Myr	-	-	-
	CSFR	< 5Myr	-	-	-
Model-TA	burst	1 – 4Myr	< 2.5Myr	-	-
	CSFR	1.5Myr<	< 5.5Myr	-	-
Model-TB	burst	< 3Myr	-	-	-
	CSFR	< 5Myr	-	-	-

ages < 9Myr, the Sc model at ages < 5Myr, and the TB model at ages < 5Myr are also consistent with the observations. At metallicity of $Z = 10^{-7}$, some models can attain $Ly\alpha$ EW_0 as high as the observed, but only in a young population with ages <2-4Myr, while none of the predicted He II EW_0 are as high as in the case $Z = 0$. Model-B and Model-C are consistent with the observations at ages <1.5Myr and ages <4Myr for the burst and CSFR models, respectively. Model-TA is consistent with the observations at ages <2.5Myr and ages <5.5Myr for the burst and CSFR models, respectively. At metallicity $Z = 10^{-5}$, the predicted He II EW_0 of all models are low enough to satisfy the observational constraint, and only Model-B and Model-C at very young ages at < 1 – 2Myr are consistent with the observed $Ly\alpha$ EW_0 . Model-S, which has an upper mass as small as $100M_\odot$, is no longer consistent with the observations at $Z > 10^{-5}$. At metallicity $Z = 10^{-3}$ and higher, no model can explain the observed large $Ly\alpha$ EW_0 .

To summarize, some IMF models with $Z < 10^{-5}$, and even $Z = 0$, can simultaneously explain the large $Ly\alpha$ EW_0 and the stringent upper limit on the He II $\lambda 1640$ EW_0 , but only over a short (\sim several Myr) age period. Among the Salpeter IMF models (S, B, and C), models with higher upper mass ($500M_\odot$; Model-B and C) are able to explain the observation over a wider range of metallicities and ages. The observed large EW_0 of $Ly\alpha$ is hardly explained by models with $Z \geq 10^{-3}$.

The models we used assume the conventional case B, which is not a good approximation for line and continuum emissions from a primordial nebula with low metallicity. The $Ly\alpha$ line is boosted by 20–40% when allowing for possible departures from case B, due to collisional effects, which increase the population of the $n=2$ level of hydrogen, leading to additional ionization, as discussed in Raiter et al. (2010). Collisional excitation would be especially significant at low metallicity below $< 0.03Z_\odot$ because of reduced radiative cooling and the consequent high electron temperature in the nebula. The maximum $Ly\alpha$ EW_0 could reach $\sim 2000\text{\AA}$ or higher at zero-metallicity when taking account of the departures from case B. In contrast, the He II EW_0 could become weaker than in case B due to its dependence on the ionization parameter and enhanced nebular continuum emission.

In addition, the IMF of a metal-poor or metal-free gas is still subject to large theoretical uncertainties. Based on simple physics, the primordial gases at the centers of

dark matter minihalos of mass $\sim 10^6M_\odot$ are condensed by molecular hydrogen cooling, becoming unstable to trigger a gravitational fragmentation with a very high typical mass of $\sim 100M_\odot$, which is elucidated by many theoretical simulations (Abel et al. 2002; Bromm et al. 2002; Yoshida et al. 2006; O’Shea & Norman 2006). The IMF models in Raiter et al. (2010) also assume extremely top-heavy IMF; however, recent calculations (e.g., Krumholz et al. 2009, Turk et al. 2009, Stacy et al. 2012) propound a more complex scenario with disk fragmentation under radiative feedback, resulting in a binary system or a small cluster of stars, with a final mass of only $\lesssim 50M_\odot$. Hosokawa et al. (2011) found that Pop III stars grow up to only $\sim 40M_\odot$ due to shut-off by radiative protostellar feedback. In Figure 5, Model-S with smaller upper mass than Model-B and C has some difficulty in explaining the observed $Ly\alpha$ and He II lines at higher metallicities. In the sense, the $Ly\alpha$ and He II lines of Pop III stars are expected to be smaller than those seen in Raiter et al. (2010), making it more difficult to consistently explain both observed line strengths at $Z > 10^{-7}$.

In this scenario, we can furthermore examine the stellar mass contributed by metal-free and poor stars using $Ly\alpha$ line luminosity. In Raiter et al. (2010), they predict the $1M_\odot$ - and $1M_\odot/\text{yr}$ - normalized $Ly\alpha$ fluxes, for burst and CSFR models, respectively. We have estimated the stellar mass composed of metal-free and poor stars by scaling these predicted $Ly\alpha$ flux to the observed $Ly\alpha$ flux, assuming all the $Ly\alpha$ flux is due to these primitive stars. The stellar mass was estimated to be the order of $10^6 - 10^7M_\odot$ at the maximum age for acceptable models consistent with observed EW_0 . This is larger than a characteristic stellar mass, $1.4 \times 10^5M_\odot$, of globular clusters (Harris 1991), and comparable to the mass of the most massive super star clusters (Kornei & McCrady 2009) or the least massive dwarf galaxies (Mateo 1998) in the local universe. Does this result suggest that this object is a building block at an early stage of galaxy formation? In this case, the star-formation would have to propagate across the galaxy faster than the metal enrichment from the exploding Pop III stars, such that the current star-formation is still made from metal-free gas. Unfortunately, more quantitative estimate of the timescale of star-formation is difficult due to the lack of its physical size measurement. Otherwise, our assumption above was incorrect, and part of the $Ly\alpha$ flux of this object could be due to normal stellar population. Ono et al. (2010) have constructed the stacked SED of a large sample of LAEs at $z = 5.7$ and 6.5 , and have determined the average stellar mass as small as $(3 - 10) \times 10^7M_\odot$ with very young ages of 1 – 3 Myr from the SED fitting including nebular emission. Pirzkal et al. (2007) have derived low stellar masses ($10^6 - 10^8M_\odot$) with very young (a few Myr) age for three faint LAEs at $5.2 < z < 5.8$ in the Hubble Ultra Deep Field (HUDF). The observational estimate of stellar mass produced by normal stellar population in high- z LAEs still allows wide mass range; therefore it is difficult to estimate how much fraction Pop III stars are dominated in this galaxy. It should be noted again that the observed $Ly\alpha$ flux is affected by dust and H I absorptions; therefore our estimate of the stellar mass just gives the lower limit.

5.2. Clumpy interstellar medium

A large Ly α EW₀ might be the result of scattering in a clumpy, dusty interstellar medium (ISM). In a clumpy ISM, Ly α photons scatter off at the edges of cold H I gas clumps, in which dust is embedded, and survive to escape from the galaxy, while continuum photons are attenuated, leading to a relative enhancement of the Ly α EW₀ (Neufeld 1991; Hansen & Oh 2006). Observational evidence has been found among evolved LAEs with large Ly α EW₀, possibly explained in terms of this mechanism by stellar population analysis (Finkelstein et al. 2008) and also supported by observations to account for the observed Ly α /H α and H α /H β line ratio (Atek et al. 2009; Scarlata et al. 2009a; Finkelstein et al. 2011b, but see Cowie et al. 2011).

It would be interesting to know whether models can reproduce the extremely large EW₀ of the Ly α emission presented in the study. Some theoretical models have attempted to address the quantitative estimate of Ly α EW₀ enhancement due to clumpy ISM, though it is challenging. Kobayashi et al. (2010) concluded that a clumpy dust distribution is required for their model in order to reasonably reproduce the Ly α luminosity function (LF), UV LF, and EW distribution of LAEs from $z = 3.1$ to 6.5. In the model of Kobayashi et al. (2010), the dust clumpiness parameter, denoted by q_d ¹⁶ was introduced and was defined as the optical depth ratio of Ly α to the continuum, which effectively reflects the interstellar dust geometry. The best-fit value of this parameter was found to be $q_d = 0.149 \pm 0.03$, implying a rather clumpy ISM distribution. Assuming that $q_d = 0.15$, the Ly α EW₀ enhancement factor, $\Gamma = \text{EW}_{\text{Ly}\alpha}^{\text{obs}} / \text{EW}_{\text{Ly}\alpha}^{\text{int}}$ attains 1.53 at maximum, which is not large enough to practically account for the observed EW₀ $\sim 900\text{\AA}$ of SDF-LEW-1 with a normal stellar population even with clumpy ISM. However, galactic-scale outflow, if present, could significantly reduce the scattering optical depth of Ly α in a low-density outflowing ISM. In the case, Γ could become as large as ~ 30 at maximum when the dust content amounts to $A_V \sim 4.5$ mag, which is, however, not likely for LAEs at $z \sim 6.5$. Dayal et al. (2011) also require a clumpy ISM to fit their model to the observed Ly α and UV LFs, enhancing the Ly α EW₀ by a factor of 1.3, and 3.7 when taking into account inflow/outflow. Although several uncertain assumptions are made in the modeling, we cannot conclusively rule out the model that SDF-LEW-1 is composed of a normal stellar population with clumpy ISM. Detailed radiative transfer simulations of the Ly α photons will be required to obtain a more quantitative estimate of Ly α EW₀ enhancement in a clumpy ISM.

5.3. AGN

An alternative origin for a large Ly α EW is a large AGN contribution, but we did not identify a C IV emission line as an apparent AGN signature. Typical values of the line ratio for radio galaxies is Ly α /C IV = 6.7 at $2 < z < 3$ (Humphrey et al. 2008), and Ly α /C IV = 8.6 at $0 < z < 3$ (McCarthy et al. 1993). The ratio is expected to be smaller to be Ly α /C IV ~ 4 in the case

¹⁶ This parameter was originally introduced by Finkelstein et al. (2008), but their definitions are slightly different from each other.

of narrow-line AGNs (Schaerer 2003), and ~ 4.76 for local Syfert galaxies (Ferland & Osterbrock 1986). These values are far inconsistent with the observed 3σ lower limit of Ly α /C IV ≥ 82.7 . In addition, the optical spectrum of SDF-LEW-1 does not reveal any signature of NV $\lambda 1240$ emission line, which is a strong high-ionization metal line indicating AGN activity. Although an AGN without accompanying strong metal-line emissions has been discovered (Hall et al. 2004), its Ly α emission is moderately broad and EW₀ = 34 \AA , that are dissimilar to SDF-LEW-1. We have also checked for possible time variability, which is one of the effective ways to identify AGN suggested by Shibuya et al. (2012). Based on the original SDF image (Kashikawa et al. 2004) with 8.4 hr of integration time, taken during the 2002-2003 period, the z' -band magnitude was measured as 27.05 ± 0.127 . Within the margin of error, this is almost identical to that used in the study (Table 1). Thus, we did not detect any apparent signatures of its variability. We conclude that SDF-LEW-1 is most likely not photoionized by an active nucleus.

5.4. Ly α blob

A large Ly α EW₀ can be naturally expected in the case of a spatially extended Ly α source, often referred to as “Ly α blob” (Steidel et al. 2000; Matsuda et al. 2004); however, the NB image of SDF-LEW-1 appears to be almost unresolved with FWHM = 1.''04 (the PSF FWHM of NB921-image is 0.''98), showing no evidence of a Ly α blob. Ouchi et al. (2009) discovered a Ly α blob at $z = 6.6$. Employing the same detection surface brightness threshold of 26.8 mag arcsec⁻² used in their work, we found that the isophotal area, which is defined as the image area above the detection threshold at the object’s position, of SDF-LEW-1 was 2.77 arcsec², which is much smaller than the 5.22 arcsec² obtained by Ouchi et al. (2009). Also, when we used the fainter detection threshold of 28.0 mag arcsec⁻² as Matsuda et al. (2004) in their systematic search for Ly α blobs, the isophotal area of SDF-LEW-1 was 6.32 arcsec² ($\sim 14\text{kpc}$ in diameter at $z = 6.5$), which is much smaller than 16 arcsec² ($\sim 30\text{kpc}$ in diameter at $z = 3.1$), critical criterion for a blob in Matsuda et al. (2004). We can conclude that SDF-LEW-1 is not a Ly α blob.

It is interesting to note that a Ly α blob sometimes (Prescott et al. 2009; Scarlata et al. 2009b) has a prominent He II emission, caused by either cooling gas accreting on the dark matter halo of the galaxy (Haiman et al. 2000; Yang et al. 2006; Latif et al. 2011), or photoionization by a hard ionizing source, such as an AGN (Yang et al. 2009) or very low-metallicity stars.

5.5. Fluorescently illuminated Ly α emission

Cantalupo et al. (2012) recently reported interesting evidence of Ly α emissions originating in fluorescently illuminated by strong radiation from the nearby hyperluminous quasar HE0109-3518 at $z = 2.4$. The sample contains several LAEs with large Ly α EW₀ $> 240\text{\AA}$, which could be boosted by fluorescent emission, irrespective of internal star formation. This could be another effective mechanism for enhancing the Ly α EW₀. However, in contrast to their observation, there is no evidence of a systematic excess of LAEs with high EW₀, steepening

$\text{Ly}\alpha$ LF, or spatially strong LAE clustering around SDF-LEW-1. Two thirds of their sample have no stellar continuum counterparts, whereas SDF-LEW-1 was actually detected in the z' -band image, though most of the z' -band flux would have been contributed by $\text{Ly}\alpha$. Depending on its internal velocity field, the emission line profile of a fluorescent $\text{Ly}\alpha$ is ideally expected to be double-peaked (Cantalupo et al. 2007; Adelberger et al. 2006), which was not identified in the spectrum of SDF-LEW-1. Finally, we did not identify apparent strong ionizing source candidates around SDF-LEW-1. The closest LAE at $z = 6.5$ is 6.1 comoving Mpc along a projection away from SDF-LEW-1 and its $f_{cont}^{phot}(0.92\mu\text{m})$ is smaller than that of SDF-LEW-1. The next closest is 8.5 Mpc away, and its $f_{cont}^{phot}(0.92\mu\text{m})$ is only twice as large. There are three i' -dropout objects (Toshikawa et al. 2012) within a separation of 10 Mpc on a projection from SDF-LEW-1, all with a rest-UV magnitude of more than -21mag . Hence, they do not seem to be strong radiation sources, if they were at $z = 6.5$. Therefore, it is very unlikely that SDF-LEW-1 is fluorescently illuminated by a nearby quasar.

6. SUMMARY AND IMPLICATIONS

We found an interesting LAE at $z = 6.538$ with an extraordinary large $\text{Ly}\alpha$ $EW_0^{int} = 872_{-298}^{+844}\text{\AA}$, which is exceptionally larger than those of other LAEs. The continuum emission of the object was actually detected in the z' -band image, and its EW_0 was reliably determined. Follow-up deep NIR spectroscopy detected neither He II $\lambda 1640$ nor C IV $\lambda 1549$ emission lines from the object. No detection of C IV convinces us that it is unlikely that the object is being photoionized by an active nucleus. It has no apparent $\text{Ly}\alpha$ blob morphology features. We obtained no positive evidence that supports the fluorescent boosting of the $\text{Ly}\alpha$ emission. The observed extremely large EW_0 of the $\text{Ly}\alpha$ emission and upper limit on EW_0 of the He II $\lambda 1640$ emission can be explained by population synthesis models favoring very young and massive metal-poor ($Z < 10^{-5}$) stars, or even Population III stars. The observed large EW_0 of $\text{Ly}\alpha$ is hardly explained by models with higher metallicities of $Z \geq 10^{-3}$. A large $\text{Ly}\alpha$ EW_0 with no He II emission can also be explained by clumpy ISM, which could enhance the $\text{Ly}\alpha$ EW_0 . We cannot draw a firm conclusion about the origin of the extremely large $\text{Ly}\alpha$ EW_0 of this object. Dedicated follow-up observations, such as deep NIR/MIR imaging to determine its age or dust content, will be required to put further constraints on its origin. It should be noted that the pre-

dicted UV continuum flux of SDF-LEW-1 is $\sim 28.2\text{ mag}$, which is likely detectable by the Hubble Space Telescope (HST) and its observation would give more accurate estimate of EW_0 .

A combination of strong $\text{Ly}\alpha$ emission and He II $\lambda 1640$ emission is the most promising indicator expected for Pop III-dominated galaxies. However, the $\text{Ly}\alpha$ emission is a resonant line with a large cross section; therefore, its radiative transfer, which is complicated by the geometry and velocity field of the ISM, IGM, and dust attenuation, can significantly alter the observed $\text{Ly}\alpha$ emission. Pop III-dominated galaxies are more likely to be found at much higher redshifts, where the observed $\text{Ly}\alpha$ flux can be significantly reduced by neutral IGM during the reionization epoch. The effect makes it complicated to apply such a diagnostic to find first galaxies. Another possible diagnostic for the Pop III-dominated galaxies is the line ratio of He II $\lambda 1640$ and H α , which could be a good indicator of the IMF (Johnson et al. 2009).

The He II emission line should be a unique signature of metal-poor and Pop III stars; however, for a single burst of star formation, the He II line is so short-lived ($< 2\text{Myr}$) that its practical detection relies on surveying large volumes. No detection of a distinct He II emission is not necessarily inconsistent with a Pop III interpretation because of its very short duration. Nonetheless, the He II $\lambda 1640$ signature is likely one of the most promising indicators of metal-free stars and will continue to be sought using future large telescopes. Detection of the He II line emitted from the first galaxies at $z \geq 8$ will be made possible (e.g., Zackrisson et al. 2011) in the next decade, with the James Webb Space Telescope (JWST) or Extremely Large Telescopes (ELTs).

We thank the referee, Steven Finkelstein, for his helpful comments that improved the manuscript. We thank Daniel Schaerer, Mark Kobayashi, Mark Dijkstra, and Masashi Chiba for their useful discussions. We are grateful to the Subaru Observatory staffs for their help with the observations. We especially thank Ichi Tanaka with help on MOIRCS observing and its data reduction. The observing time for part of this project was committed to all the Subaru Telescope builders. This research was supported by the Japan Society for the Promotion of Science through Grant-in-Aid for Scientific Research 23340050.

Facilities: Subaru (MOIRCS, FOCAS, Suprime-Cam), KeckII (DEIMOS), UKIRT (WFCAM), Spitzer (IRAC, MIPS).

REFERENCES

- Abel, T., Bryan, G.L., & Norman, M.L. 2002, *Science*, 295, 93
 Adams, J.J. et al. 2012, *ApJS*, 192, 5
 Adelberger, K.L. et al. 2006, *ApJ* 637, 74
 Atek, H. et al. 2009, *A&A*, 506, L1
 Bromm, V., Kudritzki, R.P., & Loeb, A. 2001, *ApJ*, 552, 464
 Bromm, V., Coppi, P., & Larson, R. 2002, *ApJ*, 564, 23
 Cai, Z., Fan, X., Jiang, L. et al. 2011, *ApJ*, 736, L28
 Cantalupo, S., Lilly, S., Porciani, C. 2007, *ApJ*, 657, 135
 Cantalupo, S., Lilly, S., Haehnelt, M.G. 2012, arXiv:1204.5753
 Ciardi, B., & Salvaterra, R. 2007, *MNRAS*, 381, 1137
 Cowie, L., Barger, A.J., & Hu, E. 2011, *ApJ*, 738, 136
 Dayal, P., Maselli, A., Ferrara, A. 2011, *MNRAS*, 410, 830
 Dijkstra, & M, Wyithe, J.S.B. 2006, *MNRAS*, 372, 1575
 Dijkstra, & M, Wyithe, J.S.B. 2007, *MNRAS*, 379, 1589
 Dunlop, J.S., McLure, R.J., Robertson, B.E. et al. 2012, *MNRAS*, 420, 901
 Erb, D.K., Pettini, M., & Shapley, A.E. et al. 2010, *ApJ*, 719, 1168
 Ferland, G. J. & Osterbrock, D. E. 1986, *ApJ*, 300, 658
 Finkelstein, S.L. et al. 2008, *ApJ*, 678, 655
 Finkelstein, S.L. et al. 2011a, *ApJ*, 729, 140
 Finkelstein, S.L., Cohen, S.H., Moustakas, J., Malhotra, S., Rhoads, J.E., & Papovich, C., 2011b, *ApJ*, 733, 117
 Finkelstein, S.L. et al., 2011c, arXiv:1110.3785
 Graur, O., Poznanski, D., Maoz, D. et al., 2011, *MNRAS*, 417, 916
 Gronwall, C. et al. 2007, *ApJ*, 667, 79
 Haiman, Z., Spaans, M. & Quataert, E. 2000, *ApJ*, 537, L5
 Haiman, Z., 2002, *ApJ*, 576, L1
 Haiman, Z. & Cen, R. 2005, *ApJ*, 623, 627
 Hall, P.B. et al. 2004, *AJ*, 127, 3146

- Hansen, M. & Oh, S.P. 2006, MNRAS, 367, 979
Harris, W. E. ARA&A, 29, 543
Hashimoto, T. et al. arXiv:1206.2316
Hosokawa, T., Omukai, K., Yoshida, N., & Yorke, H.W. 2011, Science, 334, 1250
Humphrey, A. et al. 2008, MNRAS, 383, 11
Ichikawa, T. et al. 2006, Proc. of SPIE, 6269, 38
Inoue, A.K. et al. 2011, MNRAS, 411, 2336
Jimenez, R. & Haiman, Z.(2006), Nature, 440, 501
Johnson, J.L. et al. 2009, MNRAS, 399, 37
Jones, T., Stark, D.P., & Ellis, R. 2012, ApJ, 751, 51
Kashikawa, N. et al. 2004, PASJ, 56, 1011
Kashikawa, N. et al. 2006, ApJ, 648, 7
Kashikawa, N. et al. 2011, ApJ, 734, 119
Kennicutt, R. C., Jr. 1998, ARA&A, 36, 189
Kobayashi, M.A.R., Totani, T., & Nagashima, M. 2010, ApJ, 708, 1119
Komatsu, E. et al. 2009, ApJS, 180, 330
Kornei, K.A. & McCrady, N. 2009 ApJ, 697, 1180
Krumholz, M.R., Klein, R.I., McKee, C.F., Offner, S.S. R. & Cunningham, A.J. 2009, Science, 323, 754
Latif, M.A., Schleicher, D.R.G., Spaans, M., & Zaroubi, S. 2011, MNRAS, 413, L33
Laursen, P., Sommer-Larsen, J., & Razoumov, A.V., 2011, ApJ, 728, 52
Leitherer, C., Robert, C., & Heckman, T.M. 1995, ApJS, 99, 173
Maddau, P. 1995, ApJ, 441, 18
Malhotra, S. & Rhoads, J.E. 2002, ApJ, 565, L71
Mateo, M.L. 1998, ARA&A, 36, 435
Matsuda, Y. et al., 2004, AJ, 128, 569
McCarthy, P.J. et al., 1993, ARA&A, 31, 639
McLinden, E.M. et al. 2011, ApJ, 730, 136
Nagao, T. et al. 2005, ApJ, 631, L5
Nagao, T. et al. 2008, ApJ, 680, 100
Neufeld, D.A. 1991, ApJ, 370, 85
Oh, S.P., Haiman, Z., & Rees, M.J. 2001, ApJ, 553, 73
Ono, Y. et al. 2010, ApJ, 724, 1524
Orsi, A., Lacey, C.G., & Baugh, C.M. 2012, MNRAS, 425, 87
O'Shea, B. & Norman, M.L. 2006, ApJ, 648, 31
Ouchi, M. et al., 2008, ApJS, 176, 301
Ouchi, M. et al., 2009, ApJS, 696, 1164
Pirzkal, N., Malhotra, S., Rhoads, J. E., & Xu, C. 2007, ApJ, 667, 49
Poznanski, D., Maoz, D., Yasuda, N. et al. 2007, MNRAS, 382, 1169
Prescott, M.K.M., Dey, A., & Jannuzi, B.T. 2009, ApJ, 702, 554
Raiter, A., Schaerer, D., & Fosbury, A.E. 2010, A&A, 523, 64
Scannapieco, E., Schneider, R., Ferrara, A., 2003, ApJ, 589, 35
Scarlata et al., 2009, ApJ, 704, L98
Scarlata et al., 2009, ApJ, 706, 1241
Schaerer, D. 2002, A&A, 382, 28
Schaerer, D. 2003, A&A, 397, 527
Shapley, A.E., Steidel, C.C., Pettini, M., Adelberger, K.L. 2003, ApJ, 588, 65
Shibuya T. et al. 2012, ApJ, 752, 114
Shimasaku, K. et al. 2006, PASJ, 58, 313
Stacy, A., Greif, T.H., & Bromm, V. 2012, MNRAS, 422, 290
Steidel, C.C., Adelberger, K.L., Shapley, A.E., Pettini, M., Dickinson, M., Giavalisco, M. 2000, ApJ, 532, 170
Tornatore, L., Ferrara, A., Schneider, R., 2007, MNRAS, 382, 945
Toshikawa, J. et al. 2012, ApJ, 750, 137
Tumlinson, J., Giroux, M.L., & Shull, J.M. 2001, ApJ, 550, L1
Tumlinson, J., Shull, J.M., & Venkatesan, A. 2003, ApJ, 584, 608
Tumlinson, J. 2006, ApJ, 641, 1
Turk, M.J., Abel, T., & O'Shea, B. 2009, Science, 325, 601
Wang, J.X. et al. 2004, ApJ, 608, L21
Yan, Y. et al. 2006, ApJ, 640, 539
Yan, Y. et al. 2009, ApJ, 693, 1579
Yoshida, N., Omukai, K., Hernquist, L., & Abel, T. 2006, ApJ, 652, 6
Zackrisson, E., Inoue, A.K., Rydberg, C-E., & Duval, F. 2011, MNRAS, 418, L104